International Journal of Hydrogen Energy 142 (2025) 654–661

Contents lists available at ScienceDirect

International Journal of Hydrogen Energy

journal homepage: www.elsevier.com/locate/he

Complete multicomponent versus mixture-averaged calculations of a laminar H_2/N_2 diffusion flame including heat transfer at the burner and Soret effects

Bertrand Naud [a,*], Manuel Arias-Zugasti [b], Alberto Cuoci [c]

[a] Modelling and Numerical Simulation Group, Energy Department, CIEMAT, Avda. Complutense 40, 28040 Madrid, Spain
[b] Departamento de Física Matemática y de Fluidos, Facultad de Ciencias Universidad Nacional de Educación a Distancia (UNED), Av. de Esparta s/n, Carretera de Las Rozas al Escorial km 5, Las Rozas, 28232 Madrid, Spain
[c] Department of Chemistry, Materials, and Chemical Engineering "G. Natta" Politecnico di Milano, Milan, Italy

ARTICLE INFO

Keywords:
Differential diffusion
Multicomponent gases
Fick diffusion
Thermodiffusion
Kinetic Theory of Gases
Mixture-averaged

ABSTRACT

The implementation of full multicomponent treatment of diffusion fluxes in the CFD solver for laminar reacting flows with detailed kinetic mechanisms `laminarSMOKE++` is presented. The optimised $1+M$ multicomponent formulation (including Fick diffusion and Soret effects) derived from the Kinetic Theory of Gases, with a similar computational cost as mixture-averaged, is considered. Results are presented for a H_2/N_2 laminar coflow diffusion flame, where either heat transfer at the burner wall is included, either the wall is considered adiabatic. We observe that full multicomponent and mixture-averaged results are very similar when Soret effects are neglected. However, differences are observed when including thermodiffusion. In particular with heat transfer at the wall, large differences are observed whether thermodiffusion is neglected or included. In this case, the mixture-averaged approximation used for the thermal diffusion coefficients leads to significant differences in the results compared to the full multicomponent $1+M$ formulation.

1. Introduction

Molecular transport is a key process in combustion. In addition to convection, it brings together reactants, products and heat, allowing or inhibiting chemical reactions. It is therefore important to correctly evaluate heat and mass diffusion fluxes, taking correctly into account the different diffusivities of heat and chemical species. In particular, hydrogen combustion involves fuel species and radicals like H_2 or H, with high diffusivities compared to larger molecules like O_2, N_2, H_2O. Moreover, in combustion processes, temperature and species concentrations are bound to vary strongly in space (inside or outside the flame region, or when different streams bring reactants together).

Full multicomponent treatment of diffusion fluxes is based on the work of Monchick and Mason who generalised the Kinetic Theory of Gases (KTG) to polyatomic molecules [1–3]. Dixon-Lewis [4,5] described molecular transport in the context of reacting flows, including Fick diffusion and thermodiffusion (the so-called Soret effect). In this case, the Fick diffusion flux of species i is expressed in terms of a sum over the N species considered, $\sum_j D_{ij}\nabla X_j$, where D_{ij} is the $N \times N$ matrix of Fick diffusion coefficients and ∇X_j is the gradient of mole fraction of species j. The thermodiffusive contribution to the diffusion flux of species i is expressed as $D_{\text{Soret,i}}\nabla \ln T$, with $D_{\text{Soret,i}}$ the thermal diffusion coefficient of species i and T the temperature. In order to obtain the Fick diffusion coefficients D_{ij}, a $N \times N$ matrix needs to be inverted. Moreover, in order to obtain the thermal conductivity λ and the thermal diffusion coefficients $D_{\text{Soret,i}}$, a $3N \times 3N$ system of linear equations must be solved. This full multicomponent formulation, including Soret effects, has mainly been used so far only in 1D calculations due to its high computational cost, in particular when N, the number of species involved, is large.

To reduce the computational time associated to the evaluation of diffusion fluxes, simplifications are usually applied in modelling multidimensional (2D and 3D) flames, for instance by modelling species diffusivities as the thermal diffusion coefficient divided by given constant Lewis numbers Le_i for each species i. This approximation is also usually used in analytical calculations, as it leads to simpler expressions for the diffusion fluxes. A more advanced model usually used to deal with multicomponent diffusion is the well known mixture-averaged (MA) approximation [6,7]. In this case, the Fick mass diffusion fluxes are simply expressed as $D_i^{(\text{MA})}\nabla X_i$ where the Fick diffusion coefficients $D_i^{(\text{MA})}$ are evaluated as a function of species concentrations and binary diffusion coefficients which depend on the temperature. Simplified versions of molecular transport usually used in combustion also include an approximation for thermal conductivity λ [8], and in some cases for the thermal diffusion coefficients $D_{\text{Soret,i}}$ (for instance, considered to be non-zero for "light" species only).

* Corresponding author.
E-mail address: bertrand.naud@ciemat.es (B. Naud).

https://doi.org/10.1016/j.ijhydene.2024.12.493
Received 30 April 2024; Received in revised form 5 December 2024; Accepted 30 December 2024
Available online 9 January 2025

Recently, a series of studies [9–11] has lead to an accurate and efficient complete multicomponent formulation [12] referred to as "1 + M formulation", offering a way to evaluate the multicomponent diffusion coefficients in agreement with the complete formulation derived from the KTG, at a similar computational cost as the mixture-averaged approximation.

In this paper, we present the implementation of the 1 + M formulation in `laminarSMOKE++`, a CFD solver for laminar reacting flows with detailed kinetic mechanisms, based on `OpenFOAM®` and `OpenSMOKE++` frameworks [13–15]. The efficiency, accuracy and easy implementation of this 1 + M formulation makes it indeed particularly interesting compared to other full multicomponent diffusion approaches [16–21].

More specifically, we present a comparison of different treatments of molecular transport: using either the mixture-averaged approximation or the complete 1 + M multicomponent transport, including or neglecting the thermodiffusive transport (Soret effect). The case considered is a H_2/N_2 laminar coflow diffusion flame, presented in [22]. Since this is a steady axisymmetric flame, 2D calculations are performed. The simulations have been carried out with the CRECK detailed kinetic mechanism [23], keeping only the species and reactions for hydrogen combustion (8 reacting species + N_2).

The objective of this study is to illustrate the difference between mixture-averaged approximation and complete multicomponent transport. In particular, we aim at showing the importance of thermodiffusive transport of species (Soret effect) in such a simple flame, depending on how heat transfer at the burner wall is considered.

2. Multicomponent diffusion coefficients

2.1. Transport properties

The single-component viscosities η_k, the binary diffusion coefficients $\mathcal{D}_{ki}$ and the approximations of pure thermal conductivities λ_k and thermal diffusion ratios θ_{ik} for "light species" i are obtained as functions of temperature T:

$$\ln \eta_k = \sum_{n=1}^{4} a_{n,k} (\ln T)^{n-1} \tag{1}$$

$$\ln \mathcal{D}_{ki} = \sum_{n=1}^{4} d_{n,ki} (\ln T)^{n-1} \tag{2}$$

$$\ln \lambda_k = \sum_{n=1}^{4} \beta_{n,k} (\ln T)^{n-1} \tag{3}$$

$$\theta_{ik} = \sum_{n=1}^{4} \alpha_{n,ik} T^{n-1} \tag{4}$$

where the coefficients $a_{n,k}$, $d_{n,ki}$, $\beta_{n,k}$ and $\alpha_{n,ik}$ are obtained as polynomial fits of the expressions for η_k, $\mathcal{D}_{ki}$, λ_k and θ_{ik} given in [5] (and summarised in the Appendix of [12]), evaluated over a given temperature range.

2.2. Mixture-averaged diffusion coefficients

The effective diffusion coefficient $D_i^{(\mathrm{MA})}$ of the ith species into the mixture is approximated as:

$$D_i^{(\mathrm{MA})} = \frac{1 - Y_i}{\sum_{k \neq i} X_k / \mathcal{D}_{ki}} = \frac{\overline{W} - W_i X_i}{\overline{W} \sum_{k \neq i} X_k / \mathcal{D}_{ki}} \tag{5}$$

where Y_i and X_i are respectively the mass fraction and mole fraction of species i, with W_i the molar weight of species i and $\overline{W}$ the molar weight of the mixture.

The thermal diffusion coefficients are considered to be non-zero for "light" species only (typically H, He and H_2). They are obtained from $D_i^{(\mathrm{MA})}$ and θ_{ik} as:

$$D_{\mathrm{Soret},i}^{(\mathrm{MA})} = \frac{W_i}{\overline{W}} D_i^{(\mathrm{MA})} \theta_{\mathrm{mix},i} \quad \text{with} \quad \theta_{\mathrm{mix},i} = \sum_k \theta_{ik} X_i X_k \tag{6}$$

Note that in this formulation the non-zero coefficients $D_{\mathrm{Soret},i}^{(\mathrm{MA})}$ for light species have negative values (while the Fick coefficients $D_i^{(\mathrm{MA})}$ are positive).

The thermal conductivity of the mixture is evaluated from [8]:

$$\lambda^{(\mathrm{MA})} = \frac{1}{2} \left[\sum_k X_k \lambda_k + \frac{1}{\sum_k X_k / \lambda_k} \right] \tag{7}$$

2.3. 1 + M main species

The 1 + M multicomponent transport formulation makes a distinction between a number $1+M$ of species labelled as "main" (non dilute) species, while the remaining $N-1-M$ species are assumed to be dilute. Thus, according to the optimised 1 + M formulation [10,12], we define locally $\mathcal{N}_M = 1 + M$ main species, where K is the species with largest molar fraction X_K, and where the other M main species verify:

$$X_i \geq \gamma X_K \tag{8}$$

with $\gamma = 10^{-5}$.

2.4. 1 + M multicomponent Fick diffusion coefficients

The matrix of Fick coefficients D_{ij}^* of dimension $N \times (N-1)$ is obtained as (with $j \neq K$):

$$D_{ij}^* = \mathcal{D}_{iK} c_{ij}, \text{ if } i \neq K \quad \text{and} \quad D_{Kj}^* = -\frac{1}{W_K} \sum_{i \neq K} W_i D_{ij}^* \tag{9}$$

where we use the same notation as in [12], $D_{ij}^* = X_i(D_{ij} - D_{iK})$, with D_{ij} as defined in [9].

According to the optimised 1 + M model, in order to obtain the matrix c_{ij} we first need to invert the $(\mathcal{N}_M - 1) \times (\mathcal{N}_M - 1)$ matrix: $\left[\mathbb{1} + \mathbb{A}_{11}\right]_{ij}^{-1}$. For main species i and j (other than species K):

$$c_{ij} = \left[\mathbb{1} + \mathbb{A}_{11}\right]_{ij}^{-1} \tag{10}$$

For dilute species:

$$c_{ii} = \frac{1}{1 + A_{22,i}} \tag{11}$$

For main species i (other than species K) and dilute species j:

$$c_{ij} = -c_{jj} \sum_{\substack{k \in \mathrm{main} \\ k \neq K}} c_{ik} A_{12,kj} \tag{12}$$

where the matrices and vectors of the Fick diffusion problem are defined as follows [9]:

1. $A_{11,ij}$ of dimension $(\mathcal{N}_M - 1) \times (\mathcal{N}_M - 1)$
2. $A_{12,ij}$ of dimension $(\mathcal{N}_M - 1) \times (N - \mathcal{N}_M)$
3. $A_{22,i}$ of dimension $(N - \mathcal{N}_M)$
4. c_{ij} of dimension $(N-1) \times (N-1)$

with:

$$A_{11,ij} = \sum_k X_k \left(\frac{\mathcal{D}_{iK}}{\mathcal{D}_{ik}} - 1 \right) \delta_{ij} + X_i \left(\frac{W_j}{W_K} - \frac{\mathcal{D}_{iK}}{\mathcal{D}_{ij}} \right) \frac{\mathcal{D}_{jK}}{\mathcal{D}_{iK}}$$

if i and j are main species (other than K)

$$A_{12,ij} = X_i \left(\frac{W_j}{W_K} - \frac{\mathcal{D}_{iK}}{\mathcal{D}_{ij}} \right) \frac{\mathcal{D}_{jK}}{\mathcal{D}_{iK}}$$

if i is a main ($i \neq K$) and j a dilute species

$$A_{22,i} = \sum_k X_k \left(\frac{\mathcal{D}_{iK}}{\mathcal{D}_{ik}} - 1 \right)$$

for dilute species i

2.5. 1 + M multicomponent thermal diffusion coefficients

For the thermodiffusion problem, the following matrices and vectors are defined:

1. $\widehat{M}_{ij}^{00,10}$ of dimension $(\mathcal{N}_M - 1) \times \mathcal{N}_M$
2. $M_{ij}^{10,00}$ of dimension $\mathcal{N}_M \times (\mathcal{N}_M - 1)$
3. $M_{ij}^{10,10}$ of dimension $\mathcal{N}_M \times \mathcal{N}_M$
4. $M_{ij}^{10,01}$ of dimension $\mathcal{N}_M \times n_M^\star$
5. $M_{ij}^{01,10}$ of dimension $n_M^\star \times \mathcal{N}_M$
6. $M_i^{01,01}$ of dimension $n_M^\star$
7. $\widetilde{a}_{10,i}$ of dimension $\mathcal{N}_M$

where $n_M^\star$ is the number of main species which are not monatomic species, and where:

$$M_{ij}^{mn,pq} = \frac{L_{ij}^{mn,pq}}{X_j} \quad \text{and} \quad \widehat{M}_{ij}^{00,10} = M_{ij}^{00,10} - \frac{W_i X_i}{W_K X_K} M_{Kj}^{00,10}$$

The matrices and vectors $L_{ij}^{00,10}$, $L_{ij}^{10,00}$, $L_{ij}^{10,10}$, $L_{ij}^{10,01}$, $L_{ij}^{01,10}$ and $L_i^{01,01}$ were detailed in the Appendix of [12]. Note that they can also be written in a slightly different way, using expressions which can be implemented more efficiently (see Supplementary Material).

As proposed in [12], the matrices are evaluated considering main species only. Moreover, we express here the thermodiffusion problem in terms of matrices $M_{ij}^{mn,pq}$ instead of $L_{ij}^{mn,pq}$. This allows to remove possible divisions by zero if dilute species are to be included in the problem.

On the other hand, since the monatomic species will always be just a few species (typically H, O, C, N, Ar, He), in order to simplify the data structure in the implementation in `laminarSMOKE++`, we will use $\mathcal{N}_M$ instead of $n_M^\star$ and fill with zeros the rows or columns corresponding to monatomic species. Instead of the components of vector $M_i^{01,01}$, we will store the inverse components $1/M_i^{01,01}$ and set their values to zero for monatomic species.

Following [11,12], the solution of the thermodiffusion problem is obtained from the vector $\widetilde{a}_{10,i}$, such that:

$$\begin{aligned} \theta_j^* &= 2.5 X_j \sum_{k \in \text{main}} M_{kj}^{10,00} \widetilde{a}_{10,k} \quad \text{for } j \neq K \\ \theta_K^* &= -\frac{1}{W_K} \sum_{j \neq K} W_j \theta_j^* \end{aligned} \tag{13}$$

$$\lambda^* = -\frac{25p}{4T} \sum_{k \in \text{main}} \left[X_k \widetilde{a}_{10,k} + \frac{X_k}{M_k^{01,01}} \left(1 - \sum_{j \in \text{main}} M_{jk}^{10,01} \widetilde{a}_{10,j} \right) \right] \tag{14}$$

where the solution vector $\widetilde{a}_{10,i}$ is approximated from Neumann series at order n (we use $n = 3$):

$$\widetilde{a}_{10,i} \approx \sum_{r=0}^{n} w_i^{(r)} \tag{15}$$

with

$$w_i^{(0)} = \frac{1}{M_{ii}^{10,10}} \left(1 - \sum_k \frac{M_{ki}^{01,10}}{M_k^{01,01}} \right) \tag{16}$$

$$\begin{aligned} w_i^{(r)} = w_i^{(r-1)} + \frac{1}{M_{ii}^{10,10}} \Bigg[&- \sum_{j \in \text{main}} M_{ji}^{10,10} w_j^{(r-1)} \\ &+ \sum_{\substack{k \in \text{main} \\ k \neq K}} \widehat{M}_{ki}^{00,10} v_{1,k}^{(r)} \\ &+ \sum_k \frac{M_{ki}^{01,10}}{M_k^{01,01}} v_{2,k}^{(r)} \Bigg] \end{aligned} \tag{17}$$

where

$$v_{1,k}^{(r)} = \sum_{\substack{\ell \in \text{main} \\ \ell \neq K}} X_\ell \frac{\mathcal{D}_{kK} c_{k\ell}}{X_k} u_{1,\ell}^{(r)} \tag{18}$$

$$u_{1,\ell}^{(r)} = \sum_{j \in \text{main}} M_{j\ell}^{10,00} w_j^{(r-1)}$$

$$v_{2,k}^{(r)} = \sum_{j \in \text{main}} M_{jk}^{10,01} w_j^{(r-1)}$$

2.6. Molecular viscosity

Both in mixture-averaged and 1 + M formulations, the molecular viscosity of the mixture μ is obtained from Wilke semi-empirical formula (modified by Bird et al.) [5]:

$$\mu = \sum_k \frac{X_k \eta_k}{\sum_\ell X_\ell \Phi_{k\ell}}$$

$$\text{with} \quad \Phi_{k\ell} = \left(1 + \sqrt{\frac{\eta_k}{\eta_\ell}} \sqrt{\frac{W_\ell}{W_k}} \right)^2 \Bigg/ \sqrt{8 \left(1 + \frac{W_k}{W_\ell} \right)} \tag{19}$$

However, in the 1 + M formulation, only the main species are included in the sums in (19), allowing to greatly reduce the cost of molecular viscosity evaluation [10,12].

3. Multicomponent diffusion fluxes

We detail here the implementation of mixture-averaged approximation and 1 + M formulation in `laminarSMOKE++`. The transport equation for mass fractions reads:

$$\frac{\partial \rho Y_i}{\partial t} + \nabla \cdot \left(\rho \mathbf{U} Y_i \right) = -\nabla \cdot \left(\rho \mathbf{V}_i Y_i \right) + \rho \dot{\omega}_i \tag{20}$$

where ρ is the density of the mixture, $\mathbf{U}$ is the convective velocity, $\mathbf{V}_i$ is the diffusion velocity of species i and $\dot{\omega}_i$ is the formation rate of species i. We focus here on the implementation of the first term on the right hand side, i.e. the divergence of the diffusion flux.

3.1. Simple Lewis number approximation

First of all, we recall here the simplest approximation for the Fick diffusion fluxes in terms of the species mass fraction gradient, based on the thermal conductivity λ:

$$\rho \mathbf{V}_i^* Y_i = -\frac{1}{\text{Le}_i} \frac{\lambda}{C_p} \nabla Y_i \tag{21}$$

where Le_i is a given constant Lewis number for species i, and C_p is the specific heat capacity of the mixture.

As explained for the mixture-averaged approximation below, the diffusion velocities $\mathbf{V}_i^*$ need to be corrected, by adding the correction velocity $\mathbf{V}_c$ defined in (23).

3.2. Mixture-averaged approximation

When using the mixture-averaged approximation, the uncorrected diffusion fluxes are written as:

$$\rho \mathbf{V}_i^* Y_i = \underbrace{-\rho \frac{W_i}{W} D_i^{(\text{MA})} \nabla X_i}_{\mathbf{j}_{\text{Fick},i}} \underbrace{-\rho D_{\text{Soret,i}}^{(\text{MA})} \nabla \ln T}_{\mathbf{j}_{\text{Soret},i}} \tag{22}$$

and a correction velocity $\mathbf{V}_c$ is added to species diffusive velocity $\mathbf{V}_i^*$ in order to ensure that the net species diffusion flux is zero:

$$\mathbf{V}_c = -\sum_j^N Y_j \mathbf{V}_j^* \tag{23}$$

In `laminarSMOKE++`, in order to implement the diffusion term in (20), we are interested in expressing the first contribution to (22) introducing the mass fraction Y_i instead of the mole fraction X_i. The

Fick diffusion flux of species i can be written:

$$\mathbf{j}_{\text{Fick},i} = -\rho D_i^{(\text{MA})} \left(1 - Y_i \frac{\overline{W}}{W_i}\right) \boldsymbol{\nabla} Y_i + \rho Y_i \overline{W} D_i^{(\text{MA})} \boldsymbol{\nabla} \left(\sum_{k \neq i} \frac{Y_k}{W_k}\right) \tag{24}$$

such that the divergence of the first term in (24) will be treated implicitly in the implementation of (20), while the other contributions will be implemented explicitly.

3.3. 1 + M formulation

For main species, the full multicomponent diffusion fluxes read:

$$\rho \mathbf{V}_i Y_i = -\rho \frac{W_i}{\overline{W}} \sum_j D_{ij}^* \boldsymbol{\nabla} X_j - \rho D_{\text{Soret,i}} \boldsymbol{\nabla} \ln T$$
$$\text{with } D_{\text{Soret,i}} = \frac{W_i}{\overline{W}} \left(\sum_j D_{ij}^* \theta_j^*\right) \tag{25}$$

For dilute species, the 1 + M formulation implies: $D_{ij}^* = D_{ii}^* \delta_{ij}$ and $\theta_j^* = 0$, such that the diffusion fluxes for dilute species read:

$$\rho \mathbf{V}_i Y_i = -\rho \frac{W_i}{\overline{W}} D_{ii}^* \boldsymbol{\nabla} X_i \tag{26}$$

No correction velocity is needed in this case.

Similar to the mixture-averaged implementation, we express the Fick diffusion fluxes in terms of Y_i, and separate the $\boldsymbol{\nabla} Y_i$ contributions, such that for main species:

$$\mathbf{j}_{\text{Fick},i} = -\rho D_{ii}^* \left(1 - Y_i \frac{\overline{W}}{W_i}\right) \boldsymbol{\nabla} Y_i + \rho Y_i \overline{W} D_{ii}^* \boldsymbol{\nabla} \left(\sum_{k \neq i} \frac{Y_k}{W_k}\right)$$
$$- \rho \frac{W_i}{\overline{W}} \sum_{k \neq i} D_{ik}^* \boldsymbol{\nabla} X_k \tag{27}$$

and for dilute species:

$$\mathbf{j}_{\text{Fick},i} = -\rho D_{ii}^* \left(1 - Y_i \frac{\overline{W}}{W_i}\right) \boldsymbol{\nabla} Y_i + \rho Y_i \overline{W} D_{ii}^* \boldsymbol{\nabla} \left(\sum_{k \neq i} \frac{Y_k}{W_k}\right) \tag{28}$$

In the 1 + M formulation, the Fick problem is reduced to a $(N-1)\times(N-1)$ matrix inversion, by removing species K from the problem. In this way, we obtain a solution where $D_{iK}^* = 0$. Note however that the $N \times N$ matrix D_{ij}^* is not unique in order to obtain the flux $\sum_j D_{ij}^* \boldsymbol{\nabla} X_j$. Since $\sum_j \boldsymbol{\nabla} X_j = \mathbf{0}$, any solution $D_{ij}^* + K_i$ will indeed give the same flux (with K_i a vector of constant values for each indice i).

Here, we are interested in maximising the diagonal diffusion coefficients D_{ii}^* that appear in the Fick diffusion terms in (27) to be implemented implicitly. In order to do so, for each main species i, we use different diffusion coefficients D_{ij}^{**} defined as:

$$D_{ij}^{**} = D_{ij}^* + D_{\text{max},i}^* \quad \text{with} \quad D_{\text{max},i}^* = \max\left(0, -D_{ij}^*\right) \tag{29}$$

By adding the modulus of the most negative value of D_{ij}^* for each main species i, we define positive diffusion coefficients D_{ij}^{**}. The coefficients D_{ij}^{**} are used instead of D_{ij}^* in (27).

4. Numerical framework and test case considered

4.1. Numerical solver

As detailed for instance in [14], `laminarSMOKE++` solves the transport equations of mass, momentum, species mass fractions and energy, assuming a Newtonian fluid. It is based on a standard `OpenFOAM®` solver (`pimpleFOAM`), modified using an operator-splitting approach in order to deal with the chemical reaction terms using detailed kinetic mechanisms. Moreover, `laminarSMOKE++` also allows to consider heat transfer between fluid and solid regions.

Besides the already available mixture-averaged approximation for the treatment of diffusion fluxes, the 1 + M full multicomponent formulation has been implemented in the solver, as described in the previous Sections.

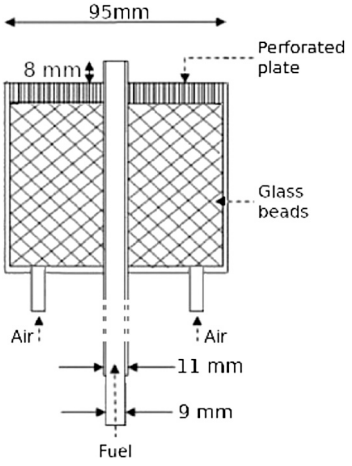

Fig. 1. Sketch of the burner studied experimentally by Toro et al. [22].

4.2. Laminar H_2/N_2 diffusion flame

The test case considered is the two-dimensional, axisymmetric, laminar hydrogen-air flame studied experimentally by Toro et al. [22], where the fuel (H_2/N_2 mixture in 1:1 mole ratio) and coflowing air streams are injected at the same bulk velocity of 50 cm/s.

The experimental burner is sketched in Fig. 1. The coflowing air passes through a perforated plate 8 mm upstream of the fuel tube exit, so that Toro et al. claim that the small jets generated by the perforated plate can relax to plug flow. The fuel pipe is long enough (455 mm) such that a fully developed parabolic velocity profile is obtained at the exit.

4.3. Numerical set-up

Computational domain. The computational domain is shown in Fig. 2. On the left hand side, the grey zone represents the fluid region of the computational domain and the black zone represents the solid region (fuel pipe wall). On the right hand side a contour of temperature (solution obtained from a full multicomponent calculation) gives a qualitative idea of the flame region in the computational domain.

Since the flame is 2D axisymmetric, the computational domain is 47.5 mm wide (half the width of the experimental burner shown in Fig. 1). The domain extends 8 mm upstream of the fuel pipe exit. A plug flow velocity condition specified at the coflow inlet boundary and a parabolic profile with the correct bulk velocity is imposed at the fuel inlet. The computational domain is 150 mm long from the fuel exit plane to the outlet.

Computational grid. Fig. 3 shows the computational grid used in the calculations (zoom on the inlet region).

A rather fine computational grid containing 26 880 cells is used (26 688 cells in the fluid region and 192 cells in the solid region). In the radial direction, 120 cells are used: 32 cells in the fuel pipe region stretched from the pipe wall towards the symmetry axis, 8 uniform cells in the wall region, and 80 cells in the coflow region stretched from the wall towards the outer lateral boundary. In the axial direction, the grid is stretched from the injector exit both downstream towards the outlet (200 cells) and upstream towards the fuel pipe inlet (24 cells). In this way, the smallest grid cells above the burner rim are 0.125 mm wide and approximately 0.065 mm long.

5. Results

Apart from [14,22], different authors have presented calculations of the flame considered here, as for instance [24–27].

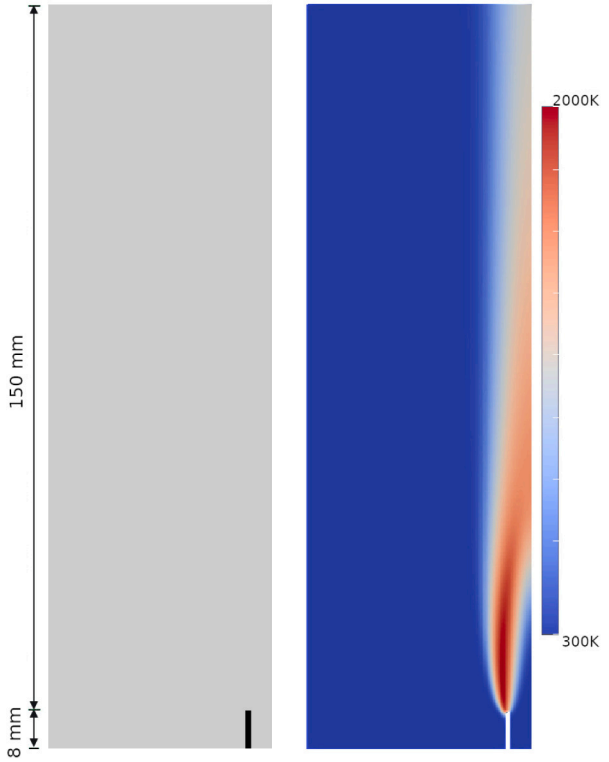

Fig. 2. Computational domain used in the calculations. On the left, fluid region of the computational domain in grey, and solid region (fuel pipe wall) in black. On the right, temperature contour from full multicomponent calculation.

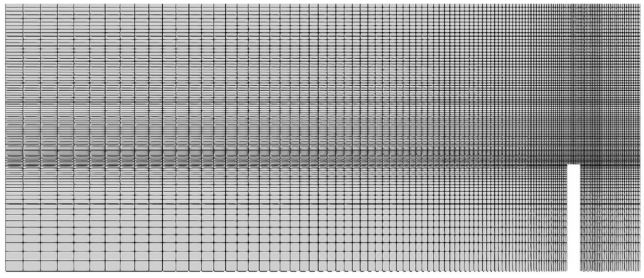

Fig. 3. Computational grid, zoom on the inlet region (full domain width).

The 9 species mechanism for hydrogen combustion obtained from the CRECK mechanism [23] is used in all the calculations discussed in the following. Two types of calculations are performed, either considering adiabatic walls, either including heat transfer at the pipe wall. In the latter case, the wall is modelled with a conductivity $\kappa = 25\text{W/(m.K)}$, and a temperature of 300 K is fixed at the fuel inlet, 8 mm upstream of the burner rim.

In all cases, the P1 radiation model is used [28]. We assume that H_2O is the only significant radiating species. The Planck mean absorption coefficient is evaluated as $a_p = p_{H_2O} a_{p,H_2O}$ where p_{H_2O} is the partial pressure of H_2O, and where the extinction coefficient a_{p,H_2O} is estimated from calculations based on the RADCAL software [29].

5.1. Adiabatic walls, comparison to 1D counterflow solutions

First of all, it is interesting to compare results from 1D calculations in the counterflow configuration, to adiabatic wall calculation results close to the injector. As in [12], the counterflow solution is obtained using the code LFLAM developed at Ciemat [30].

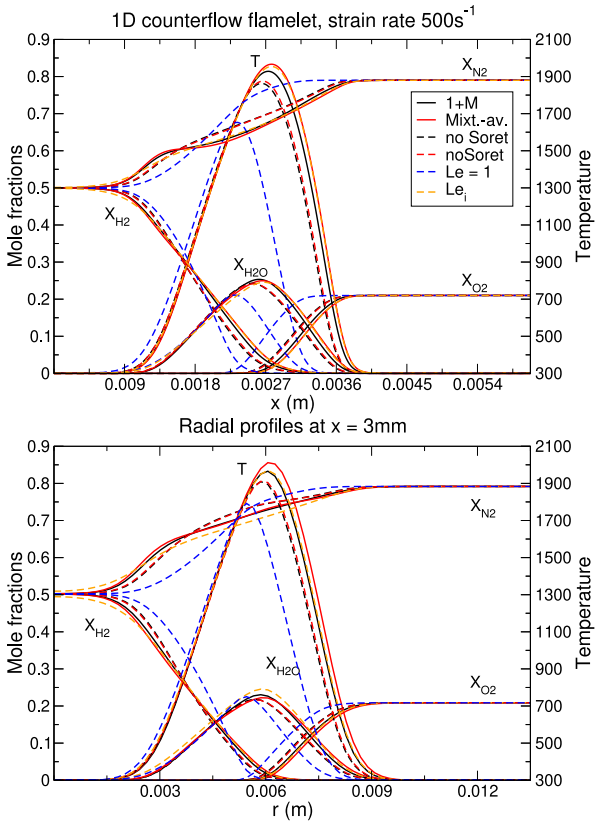

Fig. 4. Comparison of 1D counterflow results to adiabatic wall calculation results close to the injector exit. Continuous lines: including Soret effects; Dashed lines: without Soret effects. Black lines: 1 + M formulation; Red lines: mixture-averaged; Blue lines: constant Lewis number $Le_i = 1$ for all species i; Orange lines: given Lewis number Le_i for each species i (see Table 1). (For interpretation of the references to colour in this figure legend, the reader is referred to the web version of this article.)

Table 1
Imposed Lewis number Le_i for each species i when using the simple diffusion flux model (21).

H	H_2	O	OH	H_2O	H_2O_2	HO_2	O_2	N_2
0.2	0.35	0.7	0.75	0.88	1.0	1.0	1.1	1.1

In Fig. 4, we can observe that the 1D counterflow results are qualitatively similar to the adiabatic wall calculation results at 3 mm downstream of the fuel pipe exit. Without Soret effects, the 1 + M and mixture-averaged results are almost identical. When thermodiffusion is included, a higher peak temperature is predicted using the mixture-averaged approximation.

As expected, assuming a unity Lewis number for all species leads to very wrong results, as observed in [25]. On the other hand, the simple expression for the diffusion fluxes given in (21) yields reasonable results (with the constant Lewis numbers Le_i specified for each species i summarised in Table 1). Although Soret effects are not included in this case, the results with given Le_i for each species are closer to multicomponent results including thermodiffusion.

5.2. Adiabatic walls, comparison to experimental data

We compare here adiabatic wall calculation results to experimental radial profiles of temperature and N_2, O_2, H_2O and H_2 mole fractions at different downstream locations. We compare results obtained with 1 + M formulation and mixture-averaged approximation, with and without Soret effect.

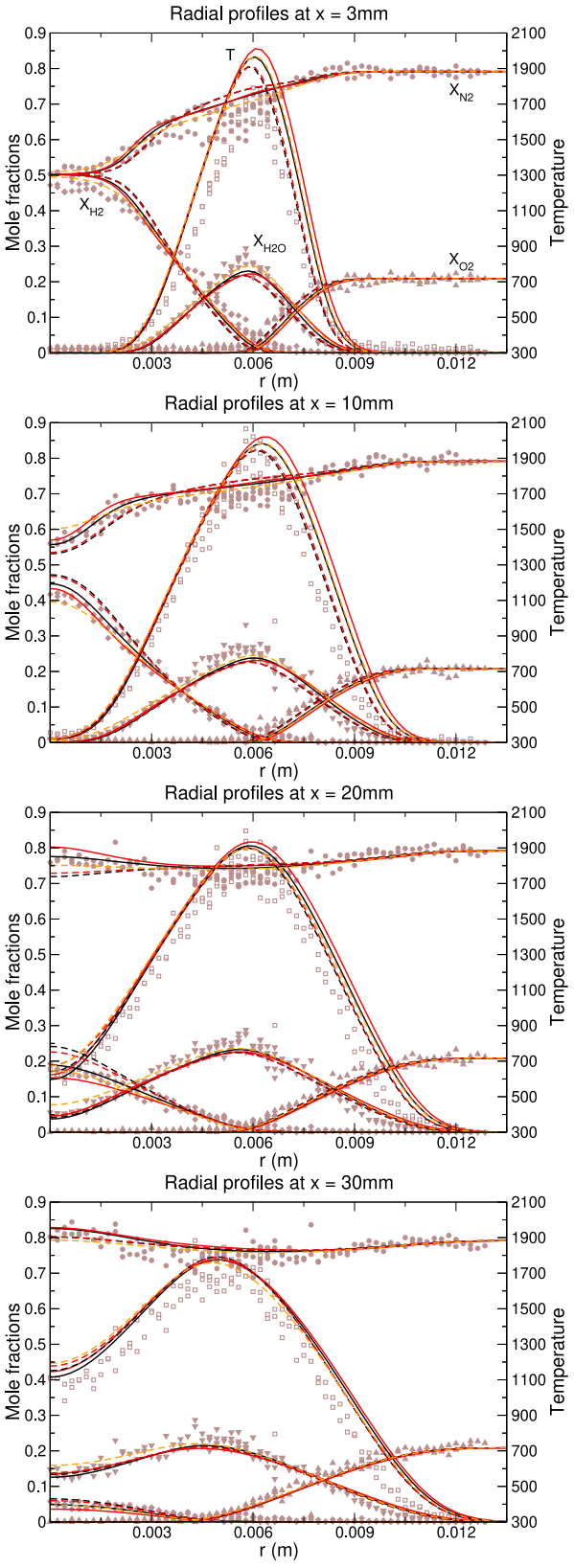

Fig. 5. Adiabatic wall calculation results. Brown symbols: experimental data. Continuous lines: including Soret effects; Dashed lines: without Soret effects. Black lines: 1 + M formulation; Red lines: mixture-averaged; Orange lines: given Lewis number Le_i for each species i (see Table 1). (For interpretation of the references to colour in this figure legend, the reader is referred to the web version of this article.)

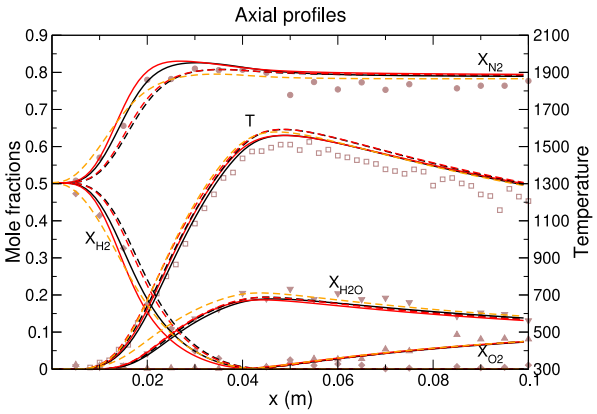

Fig. 6. Axial profiles of adiabatic wall calculations (legend see Fig. 5).

In general, we observe in Fig. 5 that the results are in good agreement with experimental data. As observed before, when thermodiffusion is not included (Soret effects neglected), the 1 + M and mixture-averaged results are almost identical at all axial locations. However, results with both diffusion flux treatments differ when thermodiffusive transport is included. The impact of thermodiffusion is particularly relevant on the centreline values of N_2 and H_2 mole fractions, showing that the diffusion of the two fuel species in the central jet is particularly affected by the flame temperature gradients. This can also be observed on the axial profiles shown in Fig. 6.

As observed in [25] with a similar approach, reasonable results are obtained with the simple expression for the diffusion fluxes given in (21). However, deviations are observed on the centreline.

5.3. Conductive walls

In Figs. 7 and 8 with conductive walls, we can observe that temperatures are now lower (and closer to experimental data), due to heat losses at the wall. The same general trends in similarities and differences between the different approaches are observed as before with adiabatic walls. Again, 1 + M and mixture-averaged results are very similar when Soret effects are neglected, and similar differences in the results are observed on the centreline.

However, we can observe in Fig. 7 that with conductive walls the Soret effects imply much larger differences in radial profiles, compared to Fig. 5 with adiabatic walls. The temperature, H_2, H_2O and O_2 radial profiles indeed appear now to be strongly affected by the different treatment of the diffusion fluxes, in particular on the lean side of the reaction zone. The largest differences are observed closer to the burner rim (at 3 mm and 10 mm downstream), where the effects of heat transfer at the wall are stronger.

We can observe that including Soret effects is particularly important in this case when heat transfer at the wall is included. Although the simple approximation of thermal diffusion coefficients (6) used with the mixture-averaged formulation has the correct qualitative impact on the results, we see that it leads to significant discrepancies compared to the 1 + M formulation derived from the Kinetic Theory of Gases.

5.4. Comparison of computational cost

In Table 2, we compare the relative computational time spent on the evaluation of the transport coefficients described in Section 2, and on the evaluation of the diffusion fluxes described in Section 3. The relative times are adimensionalised by the time spent on the chemical step and are evaluated in the adiabatic wall calculations (including Soret effects in the case of mixture-averaged and 1 + M).

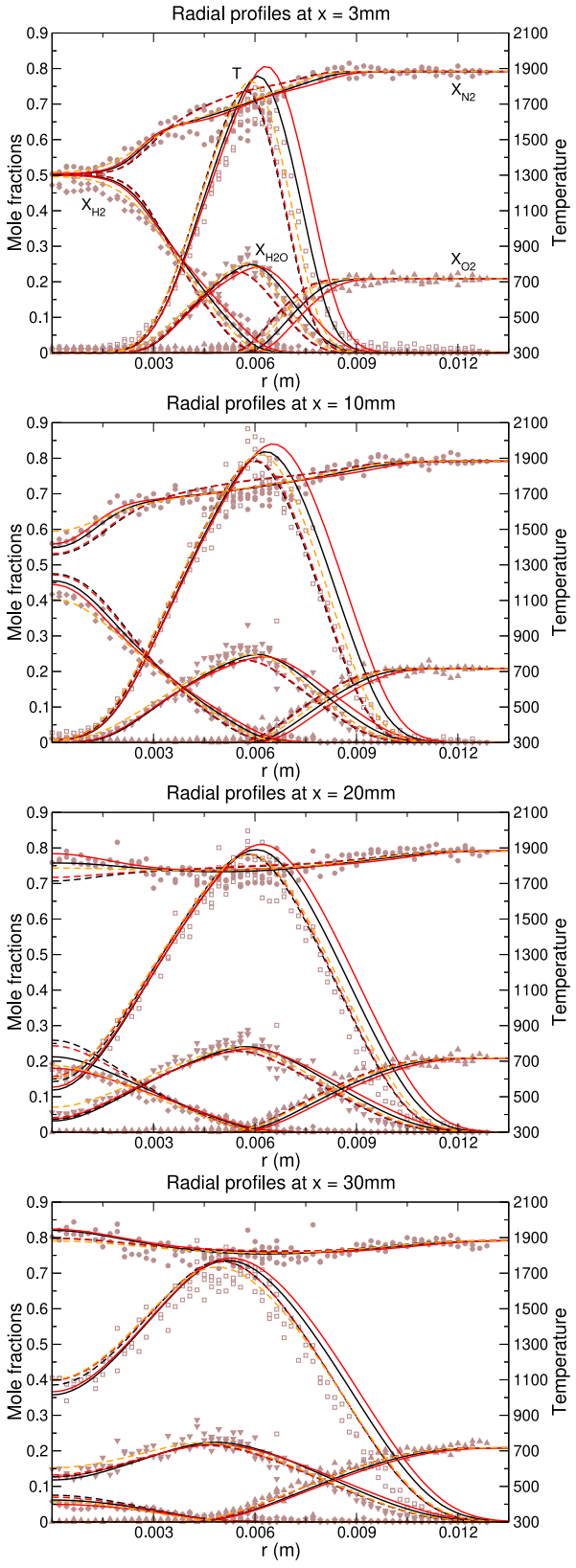

Fig. 7. Conductive wall calculation results. Brown symbols: experimental data. Continuous lines: including Soret effects; Dashed lines: without Soret effects. Black lines: 1 + M formulation; Red lines: mixture-averaged; Orange lines: given Lewis number Le_i for each species i (see Table 1). (For interpretation of the references to colour in this figure legend, the reader is referred to the web version of this article.)

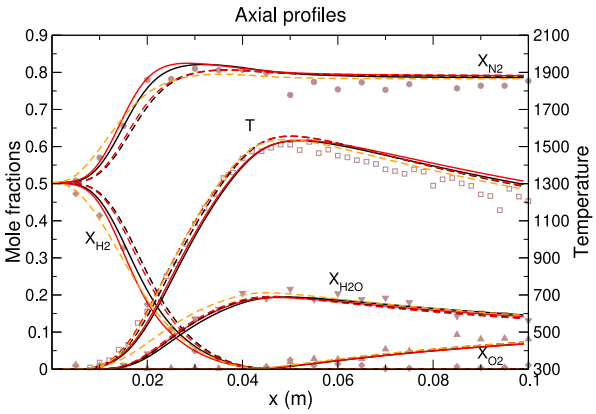

Fig. 8. Axial profiles of conductive wall calculations (legend see Fig. 7).

Table 2
Relative computational cost of given Le_i for each species, mixture-averaged and 1+M adiabatic wall calculations (including Soret effects for mixture-averaged and 1+M).

	Le_i	Mixt.-av.	1+M
Chemical reaction	1	1	1
Transport coefficients	≈0.11	≈0.15	≈0.26
Diffusion fluxes	≈0.03	≈0.05	≈0.09
Total	1.14	1.2	1.35

In this 9-species case, we see that the cost of the evaluation of both transport coefficients and diffusion fluxes in the 1 + M approximation is less than twice the mixture-averaged cost. Overall, the total cost of the calculations (including the time spent on chemical reaction) is similar.

Note that the cost of the evaluation of transport coefficients is similar with given Le_i for each species and mixture-averaged since it is dominated by the evaluation of molecular viscosity (19). The evaluation of the fluxes with given Le_i for each species is faster than with mixture-averaged, mostly because they are directly expressed in terms of mass fraction gradients (21) instead of mole fraction gradients in (24), and also because Soret effects are not included. On the other hand, the evaluation of the fluxes with 1 + M takes more time compared to mixture-averaged, because of the last term in (27) for main species.

6. Conclusions

The implementation in `laminarSMOKE++` of the optimised 1 + M formulation has been detailed. This allows to perform flame calculations with detailed chemistry, including full multicomponent treatment of the diffusion fluxes (Fick and Soret) derived from the Kinetic Theory of Gases (KTG) at a similar cost as mixture-averaged approximation.

Different treatments of the diffusion fluxes have been compared in axisymmetric calculations of a H_2/N_2 laminar coflow diffusion flame. Radiation is included in all calculations, and either the burner wall is considered adiabatic, either heat transfer at the wall is considered. In general, all the results obtained are in good agreement with experimental data.

In the adiabatic wall calculations, we have verified that close to the fuel pipe exit the results with different treatment of the diffusion fluxes are qualitatively similar to 1D counterflow flame results. We have also verified that a unity Lewis number assumption leads to large discrepancies, while specifying given Lewis numbers for each species gives reasonable results with some discrepancies on the centreline.

In both adiabatic calculations and calculations including heat transfer at the wall, we have observed that 1 + M and mixture-averaged results are very similar when thermodiffusive (Soret) effects are neglected.

When including the Soret effects in the adiabatic wall calculations, some differences mostly appear on the centreline concentrations of fuel stream species (H_2 and N_2), with differences between 1 + M and mixture-averaged results.

When heat transfer at the wall is included, larger differences have been observed whether Soret effects are neglected or included, in particular on the lean side of the reaction zone, with the largest differences close to the burner rim. In this case, the approximation of thermal diffusion coefficients used with mixture-averaged leads to significant differences compared to the 1 + M formulation derived from the Kinetic Theory of Gases.

We have verified that the overall cost of the 1 + M and mixture-averaged calculations is of the same order. Therefore, `laminarSMOKE++` now offers the possibility to perform affordable flame calculations including Fick and Soret multicomponent diffusion derived from the KTG. We have shown that this could be particularly relevant when dealing with problems including heat transfer at solid boundaries.

CRediT authorship contribution statement

Bertrand Naud: Writing – original draft, Software, Methodology, Investigation, Data curation, Conceptualization. **Manuel Arias-Zugasti:** Writing – review & editing, Methodology. **Alberto Cuoci:** Writing – review & editing, Software, Data curation.

Declaration of competing interest

The authors declare that they have no known competing financial interests or personal relationships that could have appeared to influence the work reported in this paper.

Acknowledgements

Supported by Project PID2022-139082NB-C52 granted by MCIN/AEI/10.13039/501100011033/ FEDER, UE at CIEMAT and Project PID2022-139082NB-C55 granted by MCIN/AEI/10.13039/501100011033/ FEDER, UE at UNED. The authors also acknowledge Ciemat and UNED funding for open access publishing.

Appendix A. Supplementary data

Supplementary material related to this article can be found online at https://doi.org/10.1016/j.ijhydene.2024.12.493.

References

[1] Monchick L, Mason EA. Transport properties of polar gases. J Chem Phys 1961;35:1676–97.
[2] Mason EA, Monchick L. Heat conductivity of polyatomic and polar gases. J Chem Phys 1962;36:1622–39.
[3] Monchick L, Yun KS, Mason EA. Formal kinetic theory of transport phenomena in polyatomic gas mixtures. J Chem Phys 1963;39:654–69.
[4] Dixon-Lewis G. Flame structure and flame reaction kinetics II. Transport phenomena in multicomponent systems. Proc R Soc Lond Ser A Math Phys Eng Sci 1968;304:111–35.
[5] Kee RJ, Dixon-Lewis G, Warnatz J, Coltrin ME, Miller JA, Moffat HK. A FORTRAN computer code package for the evaluation of gas-phase, multi-component transport properties. Sandia national laboratories report, SAND86-8246B, 1998.
[6] Wilke CR. Diffusional properties of multicomponent gases. Chem Eng Prog 1950;46:95–104.
[7] Hirschfelder JO, Curtiss CF, Bird RB. The molecular theory of gases and liquids. Wiley; 1954.
[8] Martur S, Tondon PK, Saxena SC. Thermal conductivity of binary, ternary and quaternary mixtures of rare gases. Mol Phys 1967;12:569–79.
[9] Arias-Zugasti M, Garcia-Ybarra PL, Castillo JL. Efficient calculation of multicomponent diffusion fluxes based on kinetic theory. Combust Flame 2016;163:540–56.
[10] Naud B, Arias-Zugasti M. Accurate multicomponent fick diffusion at a lower cost than mixture-averaged approximation: validation in steady and unsteady counterflow flamelets. Combust Flame 2020;219:120–8.
[11] Córdoba O, Arias-Zugasti M. Accurate and efficient calculation of multicomponent thermal diffusion coefficients and partial thermal conductivity based on kinetic theory. Combust Flame 2022;244:112202.
[12] Naud B, Córdoba O, Arias-Zugasti M. Accurate heat (Fourier) and mass (fick and thermodiffusion) multicomponent transport at similar cost as mixture-averaged approximation. Combust Flame 2023;249:112599.
[13] Cuoci A, Frassoldati A, Faravelli T, Ranzi E. Numerical modeling of laminar flames with detailed kinetics based on the operator-splitting method. Energy Fuels 2013;27:7730–53.
[14] Cuoci A, Frassoldati A, Faravelli T, Ranzi E. A computational tool for the detailed kinetic modeling of laminar flames: Application to C_2H_4/CH_4 coflow flames. Combust Flame 2013;160:870–86.
[15] Cuoci A, Frassoldati A, Faravelli T, Ranzi E. Comput Phys Comm 2015;192:237–64.
[16] Giovangigli V. Convergent iterative methods for multicomponent diffusion. Impact Comput Sci Eng 1991;3:244–76.
[17] Ern A, Giovangigli V. Fast and accurate multicomponent transport property evaluation. J Comput Phys 1995;406:105–16.
[18] Ern A, Giovangigli V. Multicomponent transport algorithms. Lecture notes in physcis monographs, Berlin, Heidelberg: Springer; 2008.
[19] Xin Y, Liang W, Liu W, Lu T, Law CK. A reduced multicomponent diffusion model. Combust Flame 2015;162:68–74.
[20] Ambikasaran S, Narayanaswamy K. An accurate, fast, mathematically robust, universal, non-iterative algorithm for computing multi-component diffusion velocities. Proc Combust Inst 2017;36:507–15.
[21] Sun W, Ju Y. A multi-timescale and correlated dynamic adaptive chemistry and transport (CO-DACT) method for computationally efficient modeling of jet fuel combustion with detailed chemistry and transport. Combust Flame 2017;184:297–311.
[22] Toro VV, Mokhov AV, Levinsky HB, Smooke MD. Combined experimental and computational study of laminar, axisymmetric hydrogen–air diffusion flames. Proc Combust Inst 2005;30:485–92.
[23] Bagheri G, Ranzi E, Pelucchi M, Parente A, Frassoldati A, Faravelli T. Comprehensive kinetic study of combustion technologies for low environmental impact: MILD and OXY-fuel combustion of methane. Combust Flame 2020;212:142–55.
[24] Maragkos G, Rauwoens P, Merci B. A new methodology to incorporate differential diffusion in CFD simulations of reactive flows. Combust Flame 2013;160:1903–5.
[25] Maragkos G, Rauwoens P, Merci B. Differential diffusion effects in numerical simulations of laminar, axi-symmetric H_2/N_2–air diffusion flames. Int J Hydrog Energy 2014;39:13285–91.
[26] Piemsinlapakunchon T, Paul MC. Effects of content of hydrogen on the characteristics of co-flow laminar diffusion flame of hydrogen/nitrogen mixture in various flow conditions. Int J Hydrog Energy 2018;43:3015–33.
[27] Benim AC, Korucu A. Computational investigation of non-premixed hydrogen-air laminar flames. Int J Hydrog Energy 2023;48:14492–510.
[28] Modest MF. Radiative heat transfer. 3rd ed.. Elsevier; 2013.
[29] Hall RJ. The radiative source term for plane-parallel layers of reacting combustion gases. J Quant Spectrosc Radiat Transfer 1993;49:517–23.
[30] Naud B, Novella R, Pastor J-M, Winklinger JF. RANS modelling of a lifted H_2/N_2 flame using an unsteady flamelet progress variable approach with presumed PDF. Combust Flame 2015;162:893–906.